Kovove Mater. 62 2024 129–145
DOI: 10.31577/km.2024.3.129

Orthogonal experiment and hardening mechanism investigation on the effect of heat treatment parameter on Sb-modified Mg_2Si/Al-8Si composites

Peng Tang[1,2]*, Fan Mo[1], Hao Li[1]

[1] *School of Resources, Environment and Materials, Guangxi University, Nanning, Guangxi 530004, P. R. China*
[2] *State Key Laboratory of Featured Metal Materials and Life-cycle Safety for Composite Structures, Guangxi University, Nanning, Guangxi 530003, P. R. China*

Received 23 April 2024, received in revised form 6 May 2024, accepted 17 May 2024

Abstract

The Al-Si-Mg alloy is highly popular in the aluminum industry, and the Mg_2Si/Al composites demonstrate extensive development prospects. However, the practical production of these composites still faces certain obstacles. In this study, $L_{32}(4^9)$ orthogonal experiments were conducted to systematically examine the impact of heat treatment conditions on 15% Mg_2Si/Al-8Si composites with 0.5%Sb modification. The microstructures of the as-cast alloys and heat-treated samples were studied using OM, XRD, DSC, SEM, EDS, and hardness tests. By conducting an orthogonal test, the influence of each factor was analyzed to quantify its magnitude and identify the optimal heat treatment process. The results showed that the hardness value of the alloy could be increased from 74.77 to 163.86 HV through heat treatment. Additionally, the average particle size of the initial Mg_2Si could be refined from 19.15 to 12.44 μm. Furthermore, the hardening mechanism of the heat treatment parameters was discussed in detail.

K e y w o r d s: 15%Mg_2Si/Al-8Si composites, orthogonal experiment, heat treatment, hardening mechanism

Highlights

– Among the nine factors considered in the designed orthogonal experiments, the secondary solid solution temperature and the secondary aging temperature had the greatest influence on the properties of the 0.5%Sb-metamorphosed 15%Mg_2Si/Al-8Si alloy. The heat-treated alloy exhibited significant improvements, with the hardness value increasing from 74.77 to 163.86 HV and the average particle size of the incipient Mg_2Si refining from 19.15 to 12.44 μm.

– The optimized heat treatment process involves a primary solid solution temperature of 460 ℃, a primary aging temperature of 60 min, a secondary solid solution temperature of 530 ℃, a secondary solid solution time of 60 min, quenching in a salt solution, a primary aging temperature of 180 ℃, a primary aging time of 180 min, a secondary aging temperature of 180 ℃, and a secondary aging time of 120 min.

– The structure of the alloy mainly consists of the primary Mg_2Si phase, α-Al phase, and eutectic Mg_2Si phase. The solid solution and aging treatment process helps reduce the energy required for alloy melting, influencing the dissolution and precipitation of solute atoms. This, in turn, affects the number, size, and distribution of the second phase, ultimately leading to an improvement in the hardness of the alloy.

1. Introduction

As a structural material, aluminum alloy has been widely utilized in various advanced engineering fields, including automotive, communications, aerospace, nuclear industry, and more [1–6]. However, with the advancement of human society, single traditional metal materials have struggled to keep pace with social progress. For instance, pure aluminum exhibits low

*Corresponding author: tel./fax: +86 77 13232200; e-mail address: tp@gxu.edu.cn

strength, low hardness, low melting point, and various deficiencies, making it challenging to employ directly in industrial applications. Numerous advantages of Al-Si alloy are achieved by utilizing Al-Si cast aluminum alloy as the matrix material and incorporating 15%Mg_2Si-8Si composite by adding Mg element [7]. In contrast, the Mg_2Si phase in the material serves as the strengthening phase, effectively enhancing both the hardness and wear resistance of the alloy [8]. Al-Si-Mg alloy belongs to the 6XXX series of aluminum alloys, which can be strengthened through heat treatment [9] and plastic deformation. It is regarded as one of the most extensively researched aluminum alloys. In aluminum alloy, when Si and Mg elements [10–14] are introduced into the matrix, the formation of the Mg_2Si phase occurs. Among reinforcing particles, Mg_2Si has a high Young's modulus (120 GPa) and melting point (1083 ℃), and low thermal expansion coefficient ($7.5 \times 10^{-6}\,K^{-1}$) and density ($1.99\,g\,cm^{-3}$), which makes it an excellent reinforcing phase for aluminum matrix composites [15]. The Mg_2Si phase exhibits exceptional properties, including a high elastic modulus, hardness, melting point, and low density. As an in-situ synthetic particle-reinforced aluminum matrix composite, the Mg_2Si/Al composite holds significant market potential and a promising development outlook. Mg_2Si/Al matrix composites fabricated via conventional fusion casting are created by solidifying the melt in its original position. When the Mg and Si element content is high, the primary Mg_2Si phase tends to aggregate, forming coarse particles. These particles often exhibit complex and irregular shapes, predominantly with sharp angles. Due to aggregation and growth, the primary Mg_2Si phase in the aluminum matrix tends to have an uneven distribution. Angular primary Mg_2Si particles make it susceptible to cutting through the matrix, reducing its plastic toughness and overall composite performance [16]. This is an important factor that hinders the promotion and application of Mg_2Si/Al matrix composites, thus limiting their widespread adoption in actual production.

Rare earth elements are known as "industrial monosodium glutamate" because of their active chemical properties and special electron layer arrangement, which allows them to react with most elements. The microalloying method can effectively modify the microstructure of the coarse Mg_2Si phase in the composite obtained through fusion casting by incorporating trace alloying elements into the material. Rare earth elements are added to Mg_2Si/Al matrix composites as metamorphic agents to enhance the mechanical properties of the materials by refining their structure. Rare earth elements are added to Mg_2Si/Al matrix composites as metamorphic agents to enhance the mechanical properties of the materials by refining their structure. Different rare earth elements have distinct functions in Mg_2Si/Al matrix composites. Researchers have recently conducted numerous studies investigating the mechanisms associated with various rare earth elements. Aziz Islahuddin et al. [17] discovered that adding Pr to the Al-15%Mg_2Si composite resulted in white AlSiPr intermetallic compounds forming between the primary Mg_2Si phases. Furthermore, the morphology and size of the primary Mg_2Si phase were altered by modifying the solidification and growth process of the equilibrium phase. In another study conducted by Wang Keyan et al. [18], Gd was added to the hypoeutectic Al-Mg_2Si composite. They observed that a portion of Gd reacted with Al to create the Al_3Gd phase, which acted as a heterogeneous nucleation site for α-Al. This process effectively refined the α-Al phase in the composite. In addition, the remaining portion of Gd leads to supercooling of the composition by segregating around the eutectic Mg_2Si phase. This segregation alters the growth process of the eutectic Mg_2Si phase and modifies its morphology. In a study conducted by Rozita Khorshidi et al. [19], it was discovered that adding Gd to Al-15Mg_2Si composites resulted in the formation of MgGd intermetallic compounds. The morphology of these compounds was found to be dependent on the amount of Gd added to the composite. The metamorphic effect of Gd on the Mg_2Si phase occurs by inhibiting the anisotropic growth of the primary Mg_2Si phase by adsorption toxicity. By introducing Cr into the Al-15%Mg_2Si composite, researchers found that an $Al_{13}Cr_4Si_4$ metal compound with a morphology similar to that of the primary Mg_2Si phase was created [20]. The inclusion of Al-Si-Cr compounds in the material leads to a significant increase in hardness, ultimate tensile strength, and elongation [21]. Additionally, Sb has been identified as an effective refining modifier for this material. In a study conducted by Tang Peng et al. [22], Al-11Si-9.5Mg-xSb alloys were prepared through melting casting with varying Sb content (x = 0, 0.10, 0.15, 0.30, 0.50, 0.80, 1.00). The results showed that as the Sb content increased, the shape of the second phase in the alloy transformed from coarse and irregular to small multilateral shapes. The second phase grew larger when more Sb was added, and the shape became irregular. This had a similar impact on the mechanical properties of the alloy, with a trend of change observed. The optimal metamorphic effect was achieved with the addition of 0.50 wt.% Sb.

There are numerous approaches to researching and developing aluminum alloy materials. Heat treatment is a highly effective and straightforward method for improving the coarse microstructure of Mg_2Si/Al composite materials. It can enhance the size, distribution, and quantity of the microstructure in the alloy, thereby enhancing its comprehensive properties and process properties. By implementing an appropriate heat treatment process, the alloying elements

Table 1. Chemical composition of alloy raw materials

Raw materials	Mass fraction (%)					
	Si	Sb	Mg	Fe	Impurities	Al
Al-20Si	19.54	–	–	0.47	0.10	Bal.
Mg	–	–	99.85	0.02	0.08	–
Al-10Mg	–	–	9.65	0.10	0.10	Bal.
Al-5Sb	–	4.98	–	0.01	0.01	Bal.

within Mg_2Si/Al matrix composites can be evenly distributed, leading to an optimized microstructure for the composites [23]. Various heat treatment processes are commonly employed to enhance the mechanical properties of Al-Mg-Si alloys [24]. Li Zedi et al. [25] discovered that by subjecting Al-10%Mg_2Si composite to T6 heat treatment, the eutectic Mg_2Si structure changed. It was broken down, spheroidized, and transformed from long rod-like structures into short fibrous and spherical formations. Simultaneously, during the T6 heat treatment, a significant quantity of β'' particles, characterized by dendrites smaller than 20 nm, were precipitated within the aluminum matrix. The thinning of the eutectic structure and the precipitation of nanoparticles have a significant impact on the tensile strength of the alloy, leading to a substantial increase in its strength. Malekan A. et al. [26] conducted a detailed study on the solid solution temperature of Al-15%Mg_2Si. Within the temperature range of 300 to 580 ℃, the microstructure of both primary Mg_2Si and eutectic Mg_2Si undergoes changes as the temperature increases. The angular bulges in the primary Mg_2Si phase gradually become deactivated, while the dendritic eutectic Mg_2Si microstructure transforms into short rod-like structures. These alterations contribute to an improvement in the tensile properties of the composites. However, if the solution temperature surpasses 580 ℃, the material becomes overburned, decreasing the tensile strength. Zhen L. et al. [27] performed a two-stage aging process on Al-1.11%Si-0.62%Mg alloy and discovered that pre-aging (80–170 ℃) can effectively hinder natural aging while enhancing the baking effect. This, in turn, leads to improvements in hardness and yield strength during the final aging stage. The solid solution treatment must be carefully controlled to ensure the complete integration of the strengthening phase and prevent grain coarsening and overburning, as these factors can significantly affect the subsequent aging treatment. Hence, studying the solution and precipitation mechanisms of various heat treatment processes is of utmost importance to meet the requirements of practical engineering applications.

Orthogonal testing allows a select number of representative experiments to represent a larger set of experiments. This approach enables the scientific arrangement and analysis of multi-factor experiments, facilitating the drawing of scientifically sound conclusions. In multi-factor analysis, the orthogonal test method is proven to yield precise analysis results while requiring fewer experimental designs. The heat treatment process variations can have varying degrees of impact on the overall properties of materials. In the case of 6XXX series aluminum alloy, the solution treatment step is crucial in the heat treatment process. In this experiment, the hardness value and average particle size of primary Mg_2Si were selected as evaluation criteria. The objective was to optimize the heat treatment process of a 15%Mg_2Si/Al-8Si alloy modified with 0.5%Sb element. This alloy combines the reinforcement properties of the Mg_2Si phase with the excellent properties of Al-Si alloy. The optimization was carried out using a nine-factor and four-level orthogonal test. The hardening mechanism of Al-Si-Mg alloy was also explored and analyzed.

2. Materials and methods

In this experiment, high-purity industrial magnesium (99.70 % purity), Al-20Si intermediate alloy, Al-5Sb intermediate alloy, and Al-10Mg intermediate alloy were utilized as the raw materials. These materials were used to synthesize a 15%Mg_2Si/Al-8Si alloy, which was further modified with 0.5%Sb. Compositional testing was carried out using an American thermoelectric direct reading spectrometer ISPARK8860 to determine the alloy composition, and the specific composition of the alloy is shown in Table 1. When designing the orthogonal experiment in this study, nine factors were taken into account and denoted as A to I. These factors included primary solution temperature (A), primary solution time (B), secondary solution temperature (C), secondary solution time (D), quenching medium (E), primary aging temperature (F), primary aging time (G), secondary aging temperature (H), and secondary aging time (I). For each factor, four levels were considered. The specific influencing factors and their corresponding levels are presented in Table 2. An orthogonal experiment scheme with nine factors and four levels was designed using the orthogonal design assistant software. The orthog-

Table 2. Factors and levels of $L_{32}(4^9)$ orthogonal experiment

Factor / Level	A (℃)	B (min)	C (℃)	D (min)	E	F (℃)	G (min)	H (℃)	I (min)
1	400	30	490	30	water	120	60	150	60
2	420	45	510	45	oil	140	120	165	120
3	440	60	530	60	salt solution	160	180	180	180
4	460	75	550	75	alkali solution	180	240	195	240

Table 3. Results of orthogonal test scheme for as-cast alloy and heat treatment

No.	A (℃)	B (min)	C (℃)	D (min)	E	F (℃)	G (min)	H (℃)	I (min)	Hardness HV	Particle size (μm)
0#	–	–	–	–	–	–	–	–	–	74.77	19.15
1#	400	30	490	30	water	120	60	150	60	96.58	18.01
2#	400	45	510	45	oil	140	120	165	120	113.60	16.59
3#	400	60	530	60	salt solution	160	180	180	180	163.86	13.81
4#	400	75	550	75	alkali solution	180	240	195	240	138.90	14.88
5#	420	30	490	45	oil	160	180	195	240	118.86	13.84
6#	420	45	510	30	water	180	240	180	180	137.50	15.09
7#	420	60	530	75	alkali solution	120	60	165	120	127.70	13.48
8#	420	75	550	60	salt solution	140	120	150	60	122.02	16.46
9#	440	30	510	60	alkali solution	120	120	180	240	150.66	14.79
10#	440	45	490	75	salt solution	140	60	195	180	109.66	14.04
11#	440	60	550	30	oil	160	240	150	120	157.36	16.29
12#	440	75	530	45	water	180	180	165	60	151.62	14.17
13#	460	30	510	75	salt solution	160	240	165	60	145.08	14.10
14#	460	45	490	60	alkali solution	180	180	150	120	144.82	12.44
15#	460	60	550	45	water	120	120	195	180	145.96	15.17
16#	460	75	530	30	oil	140	60	180	240	148.44	14.69
17#	400	30	550	30	alkali solution	140	180	165	180	134.70	16.54
18#	400	45	530	45	salt solution	120	240	150	240	132.50	15.53
19#	400	60	510	60	oil	180	60	195	60	131.76	14.86
20#	400	75	490	75	water	160	120	180	120	128.58	16.03
21#	420	30	550	45	salt solution	180	60	180	120	140.82	14.36
22#	420	45	530	30	alkali solution	160	120	195	60	131.56	15.83
23#	420	60	510	75	water	140	180	150	240	112.38	16.34
24#	420	75	490	60	oil	120	240	165	180	101.64	18.18
25#	440	30	530	60	water	140	240	195	120	136.50	15.77
26#	440	45	550	75	oil	120	180	180	60	141.78	16.82
27#	440	60	490	30	salt solution	180	120	165	240	124.18	16.49
28#	440	75	510	45	alkali solution	160	60	150	180	114.00	16.31
29#	460	30	530	75	oil	180	120	150	180	127.58	16.23
30#	460	45	550	60	water	160	60	165	240	132.90	16.65
31#	460	60	490	45	alkali solution	140	240	180	60	118.84	15.80
32#	460	75	510	30	salt solution	120	180	195	120	120.50	14.45

onal table can be denoted as $L_{32}(4^9)$, where n represents the total number of experiments, r represents the number of levels of each factor, and m represents the number of factors participating in the experiment. In this study, the Vickers hardness value and the average particle size of primary Mg_2Si were used as orthogonal evaluation indexes.

The 15%Mg_2Si/Al-8Si alloy modified by 0.5%Sb was prepared using the traditional fusion casting method. The smelting process took place in a resistance furnace with the model SG2-7.5-10, and the specific experimental process is illustrated in Fig. 1. After the casting process, the rod sample has a size of ø 25 × 130 mm^2. After the casting process is completed and the sample is completely cooled, the sample number is cut out using the Struers manual cutting machine model Labotom-15. The samples are sequentially numbered, and the corresponding heat treatment is conducted in a box furnace based on Table 3. Subsequently, the metallographic samples are prepared. The metallographic samples are subjected to corrosion using a 0.5%HF solution for 8–10 s, fol-

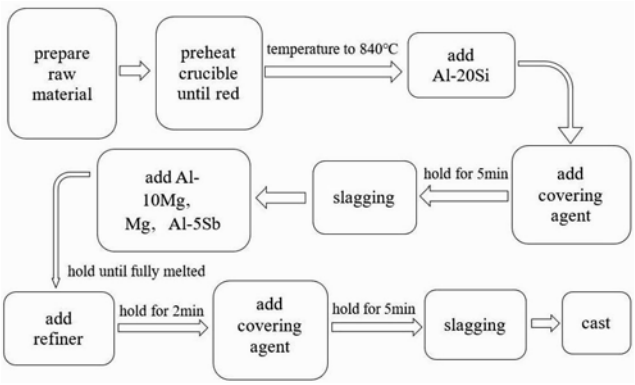

Fig. 1. Flow chart of melting and casting process.

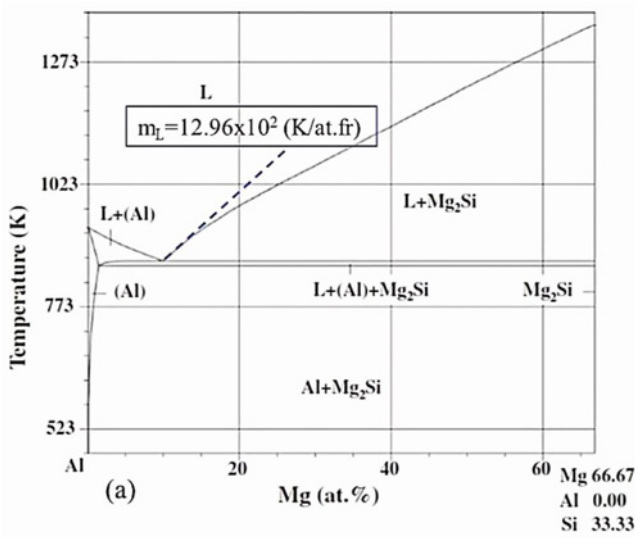

Fig. 2. Phase diagram of Al-Si-Mg system.

lowed by rinsing and blow-drying. Optical observation and metallographic photographs can be taken using the Axio Observer A1m Zeiss metallographic microscope. Finally, the Vickers hardness was measured using an HVS-1000Z digital display microscope manufactured by Shanghai Zhongyan Instrument Factory. The test was conducted under a test force of 1 kgf for a loading time of 15 s. Any points with significant deviations in each sample were removed to ensure accuracy. The remaining 10 readings were then taken as the hardness value of the sample. For X-ray diffraction analysis (XRD), the D/Max-2400 powder X-ray diffractometer was utilized with a CuKα target. The test voltage was 40 KV, and the current was 30 mA. The scanning speed for the analysis ranged from 10° to 90°, with a rate of 10 degrees per minute. The micro-morphology of the alloy was observed using the Hitachi TM4000 Plus bench scanning electron microscope (SEM). Additionally, the composition of the alloy was analyzed using the IXRF system 550i EDS spectrometer. In addition, the STA 449 F5 Jupiter Netzsch synchronous thermal analyzer was used to conduct a differential scanning calorimetry (DSC) test. The test was performed in a nitrogen-protected gas environment. For the experiment, an Al_2O_3 crucible was selected as the container. The temperature scanning range for the DSC test was set from room temperature 25 to 800 ℃. The heating rate used during the test was 10 K min^{-1}.

3. Results and discussion

3.1. Orthogonal test visual analysis

The eutectic phases of the AlSiMg alloy are Al solution (α-Al), Si, and the intermetallic Mg_2Si solution phase (see Fig. 2) [28]. It demonstrates the relationship between the composition of the alloy and its solidification path. The solidification order of the 15%Mg_2Si/Al-8Si alloy with 13.5 wt.% of Si can be represented by Eq. (1) [29]:

$$L \rightarrow L_1 + (Mg_2Si)_P \rightarrow (Si + Mg_2Si)_E \rightarrow (Al + Si + Mg_2Si)_E\,, \quad (1)$$

where the subscripts P and E in the statement denote the primary and eutectic phases, respectively. The Mg_2Si content of 15 % in the alloy exceeds its pseudo-binary eutectic point by 13.9 wt.%, categorizing it as a per-eutectic alloy. During the per-eutectic solidification process, Mg_2Si is initially formed as the incipient phase. As the solidification progresses, the eutectic phases, such as the Mg_2Si phase and the α-Al phase, are precipitated [30]. The microstructures of the as-cast pristine alloy (0#) and the alloys (1#–32#) under various heat treatment experimental protocols are depicted in Fig. 3. It is evident from Fig. 3 that the 0.5%Sb-metamorphosed 15%Mg_2Si/Al-8Si alloys predominantly comprise a white α(Al) matrix, black β-phase (Mg_2Si), and grey $\alpha + \beta$-phase (Mg_2Si). After the solid solution treatment, the alloy undergoes a process where the low melting point phases dissolve into the matrix, reducing the microscopic segregation in the cast state structure. Subsequently, during the aging treatment, the second phases gradually precipitate in the matrix and hinder the movement of dislocations. Based on Fig. 3, it is evident that the particles in the heat-treated specimens exhibit significant spheroidization compared to the original samples. Furthermore, different heat treatment processes result in varied shapes, sizes, and distributions of the α and β phases within the alloys. As a result, the material's hardness increases, and its properties become distinct.

In this experiment, the data from orthogonal tests are processed using a simple, easy, and intuitive anal-

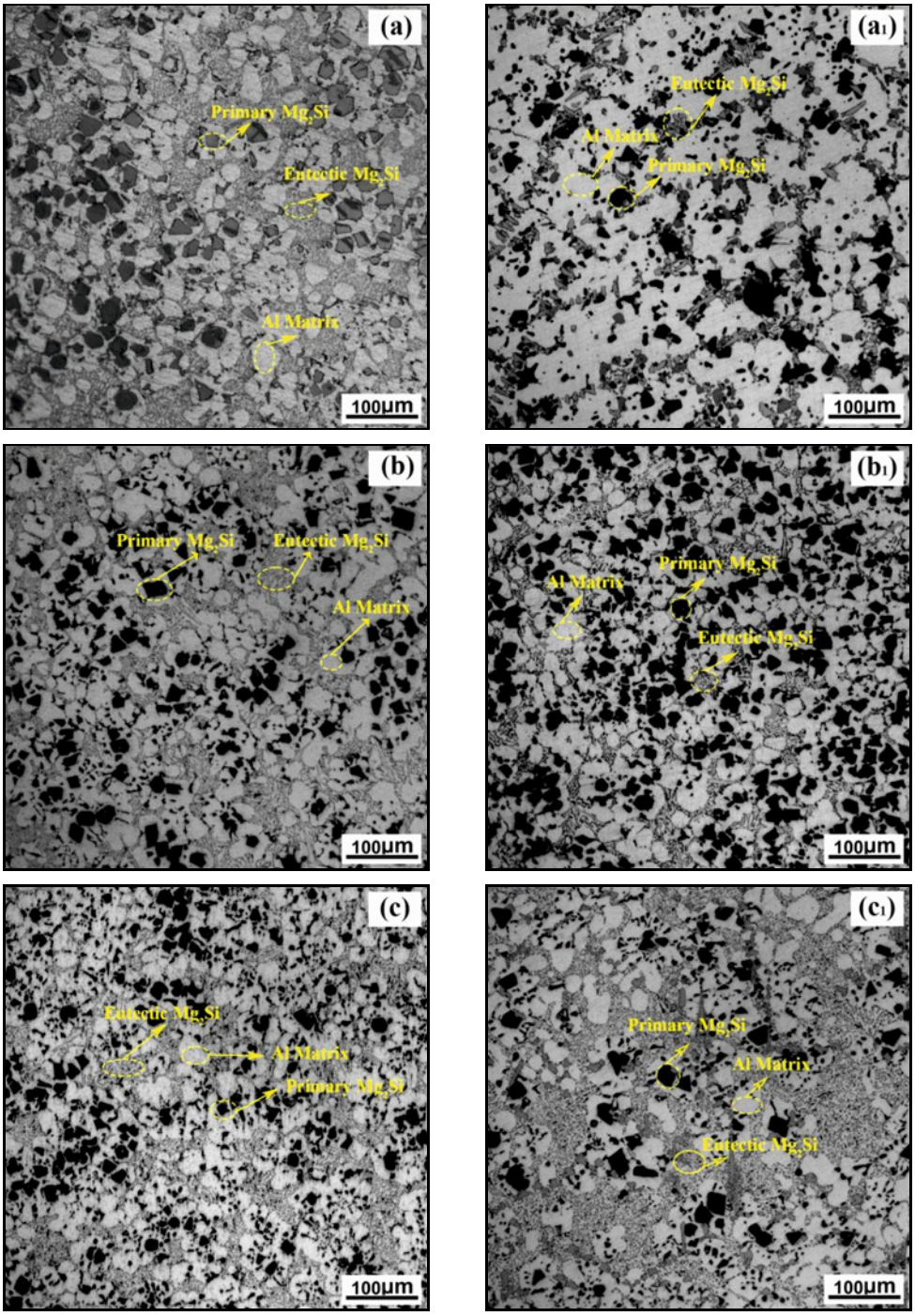

Fig. 3a. Optical microstructure of as-cast alloy and different heat-treated alloy: Original cast sample.

ysis method known as the method of polar deviation. The intuitive analysis approach helps address two main issues: determining the magnitude of the effect of each factor on the index and identifying the optimal level of each factor. This method provides a general and intuitive way of analyzing the data. In the experiment, the nine factors are denoted as A, B, C, D, E, F, G, H, and I, which correspond to primary solid solution temperature, primary solid solution time, secondary solid solution temperature, secondary solid solution time, quenching medium, primary aging temperature, primary aging time, secondary aging temperature, and secondary aging time, respectively. Each factor has four levels represented by the numbers 1, 2, 3, and 4. The range of a factor can be determined by calculating the difference between its maximum and minimum average values across all levels, as expressed by Eq. (2) [31]:

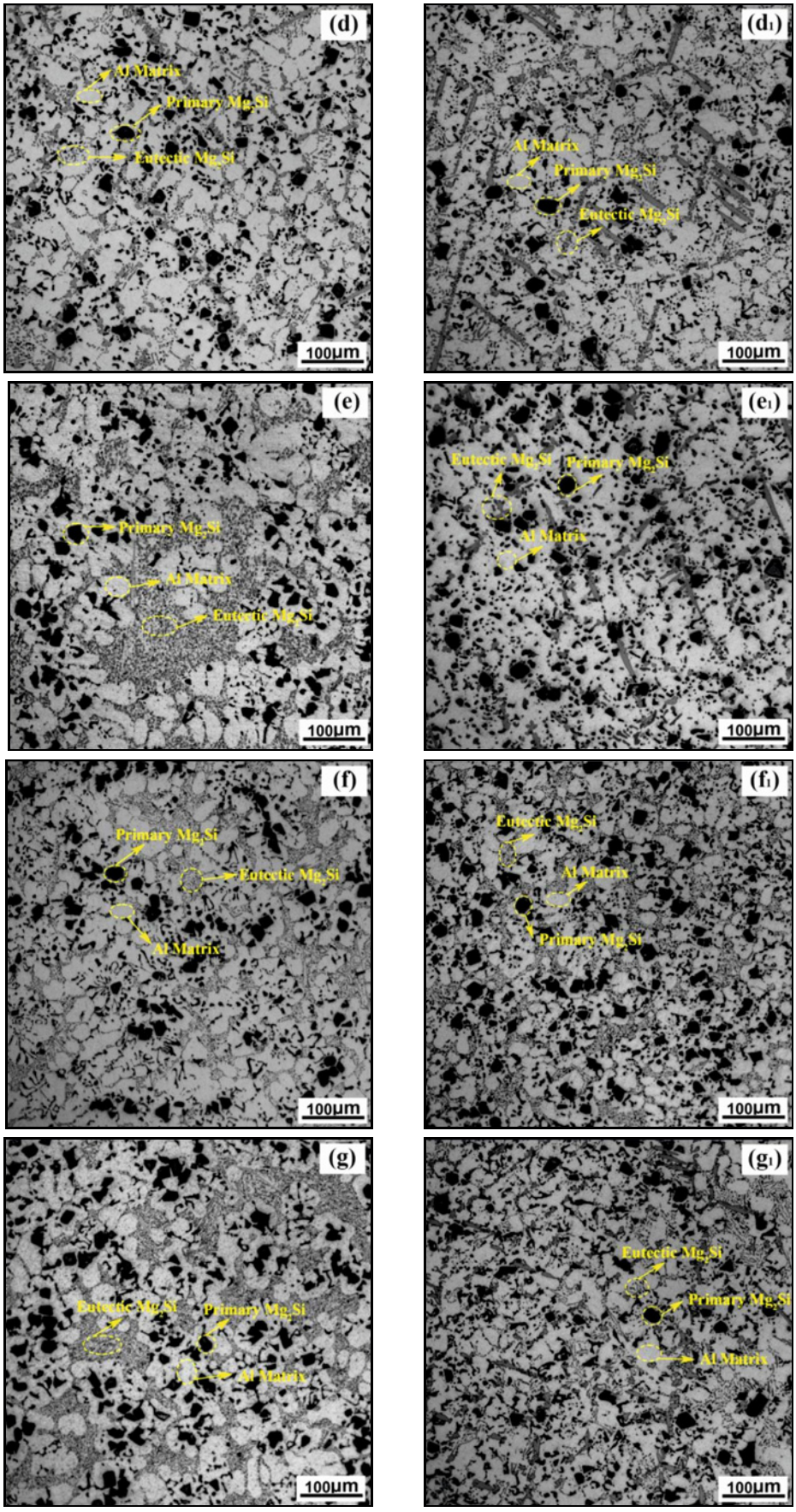

Fig. 3b. Optical microstructure of as-cast alloy and different heat-treated alloy: Original cast sample.

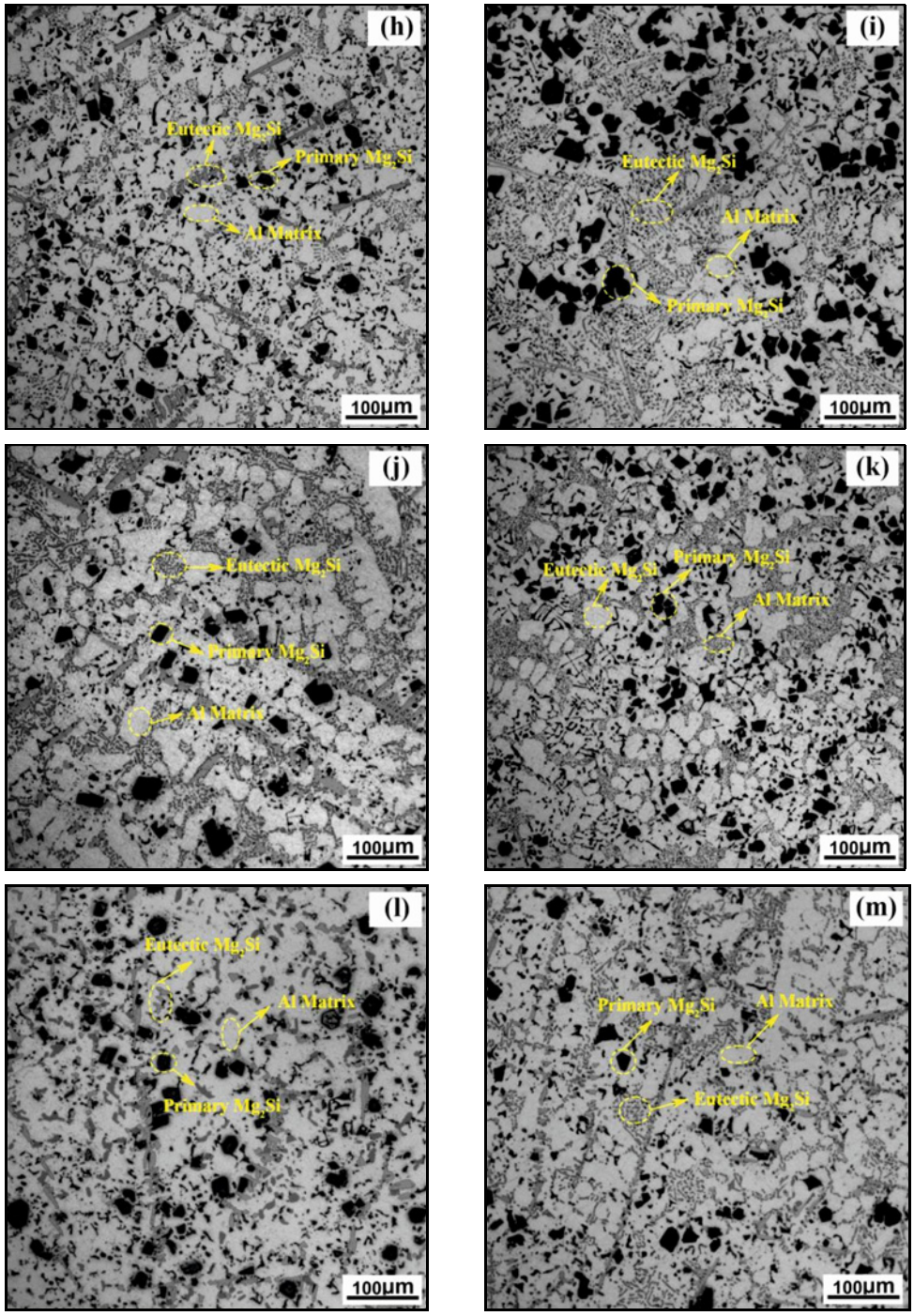

Fig. 3c. Optical microstructure of as-cast alloy and different heat-treated alloy: Heat-treated 1#–32# specimens in turn.

$$\begin{cases} K_{ab} = \dfrac{1}{l}\displaystyle\sum_{b=1}^{l} y_{ab} \\ \overline{R}_j = \max(K_{ab}) - \min(K_{ab}) \end{cases} \tag{2}$$

where K_{ab} is the average value of the corresponding experimental index y_{ab} when the factor is a and the level is b, and l denotes the factor's level number. The experimental program was conducted following the specifications in Table 2. Hardness values and the average particle size of incipient Mg_2Si were measured for each group of specimens in the orthogonal test. The experimental results obtained were recorded and are provided in Table 3. Based on Eq. (2), the experimental results were analyzed using the analysis of variance (ANOVA) method to calculate the sum of the factors at different levels. Subsequently, the extreme variance of each factor was determined based on the calculated sums. The results of this analysis are presented in Table 4. After heat treatment, the hardness

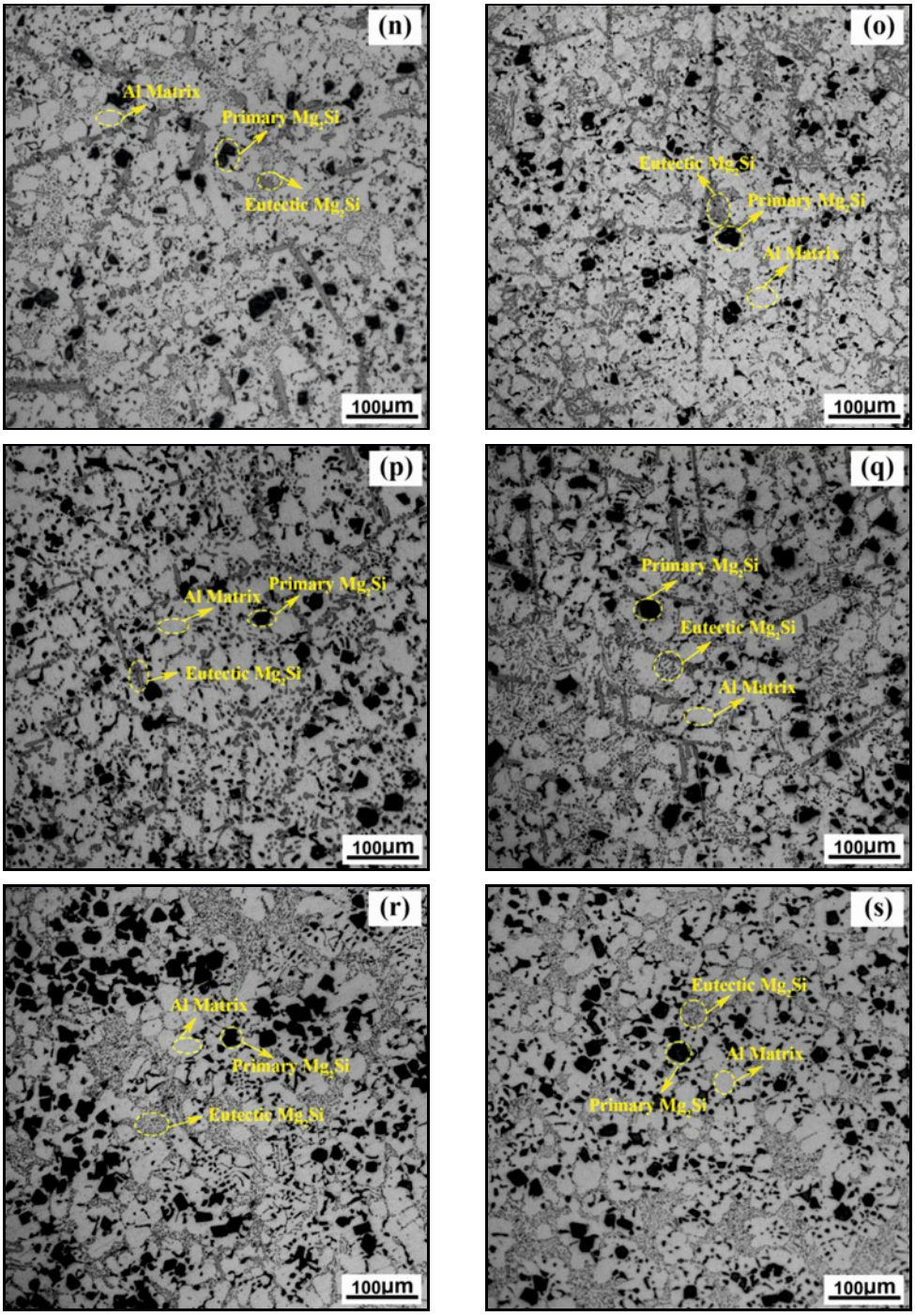

Fig. 3d. Optical microstructure of as-cast alloy and different heat-treated alloy: Heat-treated 1#–32# specimens in turn.

value of the 0.5%Sb-metamorphosed 15%Mg_2Si/Al-8Si alloy can be increased from 74.77 to 163.86 HV. Additionally, the average particle size of its incipient Mg_2Si can be reduced from 19.15 to 12.44 μm through the heat treatment process.

In the visual analysis of orthogonal tests, the magnitude of the extreme difference value for an indicator reflects the impact of a factor on that indicator. A larger extreme difference value suggests that the factor has a greater influence on the indicator and is typically considered a primary factor. Conversely, a smaller extreme difference value indicates a smaller impact and such factors are typically considered secondary factors. In this experiment, the hardness value and the primary Mg_2Si particle size are considered as the indices of heat treatment effectiveness. Higher hardness and smaller primary Mg_2Si particle size indicate a better heat treatment effect. By comparing the sums of different levels under each factor, the level number corresponding to the highest hardness value is

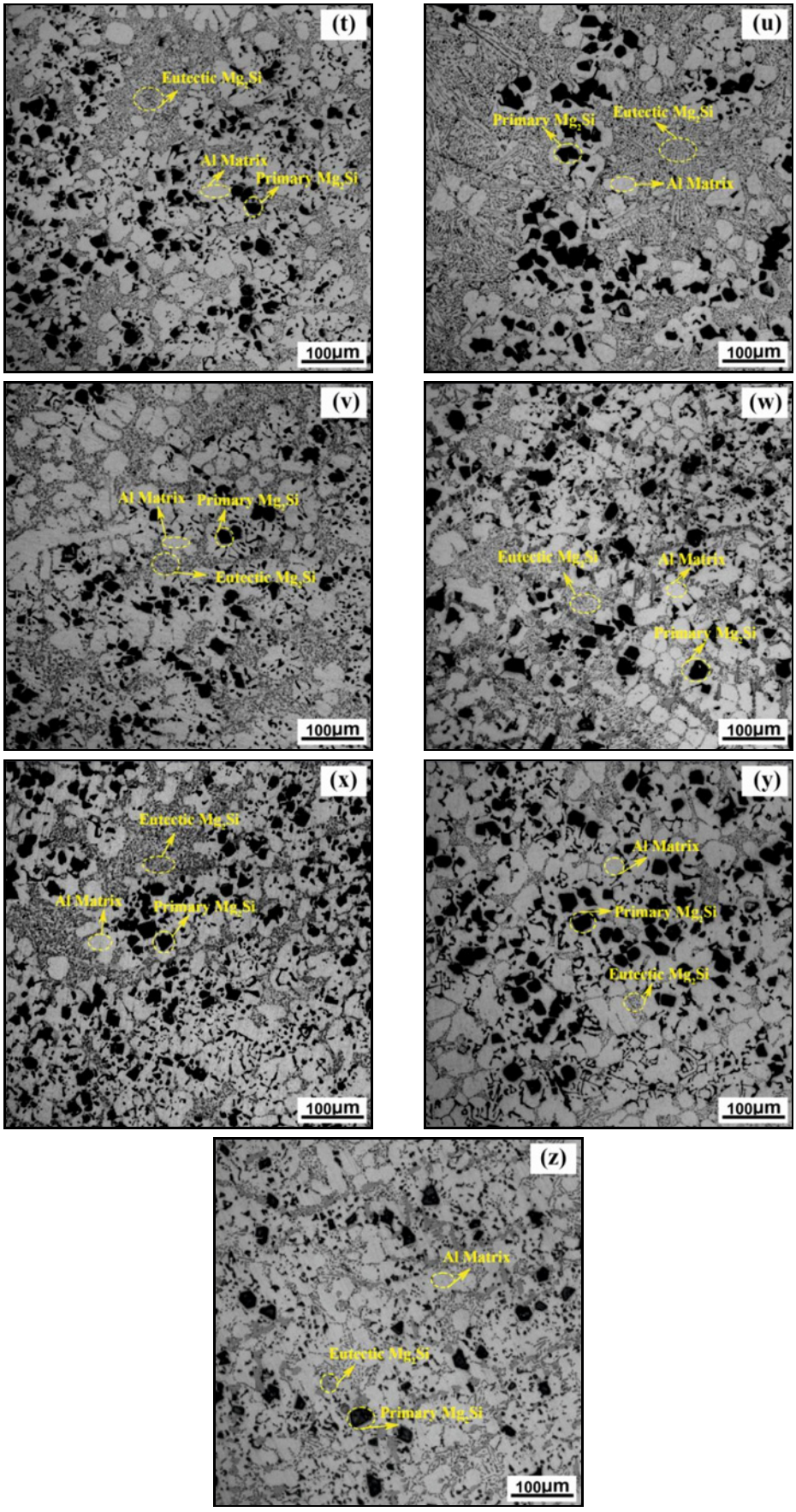

Fig. 3e. Optical microstructure of as-cast alloy and different heat-treated alloy: Heat-treated 1#–32# specimens in turn.

Table 4. Range analysis table

	Parameters	A	B	C	D	E	F	G	H	I
Hardness	k_1	130.06	131.35	117.90	131.35	130.25	127.17	125.23	125.91	129.91
	k_2	124.06	130.54	128.19	129.53	130.13	124.52	130.52	128.93	133.74
	k_3	135.72	135.26	139.97	135.52	132.33	136.53	136.07	141.31	129.36
	k_4	135.52	128.21	139.31	128.96	132.65	137.15	133.54	129.21	132.35
	$\overline{R}_j$	11.66	7.04	22.08	6.56	2.52	12.63	10.83	15.41	4.37
Particle size	k_1	15.78	15.46	15.60	15.92	15.90	15.80	15.30	15.95	15.76
	k_2	15.45	15.37	15.32	15.22	15.94	15.78	15.95	15.78	14.93
	k_3	15.59	15.28	14.94	15.37	14.91	15.36	14.80	15.17	15.67
	k_4	14.94	15.65	15.90	15.24	15.01	14.82	15.71	14.86	15.40
	$\overline{R}_j$	0.84	0.37	0.96	0.70	1.03	0.99	1.15	1.10	0.83

considered the optimal level for that factor, while the level number corresponding to the smallest primary Mg_2Si particle size is considered the optimal level for that factor. Based on the findings presented in Table 4, Figs. 4 and 5 display the polar plots illustrating the impact of each factor on the hardness value and the average particle size of incipient Mg_2Si, as well as the trend of this effect. The comprehensive balance method was utilized to statistically analyze the orthogonal test results using a single index, namely the hardness value. The analysis revealed that the nine factors have an impact on the hardness value in the following order: $C > H > F > A > G > B > D > I > E$. Using the hardness value as the evaluation index, the optimal levels for each factor were determined to be: $A_3B_3C_3D_3E_4F_4G_3H_3I_2$. This indicates that the first solid solution temperature should be 440 ℃, the first aging temperature should be 60 min, the second solid solution temperature should be 530 ℃, the second solid solution time should be 60 min, the quenching medium should be an alkaline solution, the first aging temperature should be 180 ℃, the first aging time should be 180 min, the second aging temperature should be 180 ℃, and the second aging time should be 120 min. The order of magnitude of the influence of the nine factors on the average particle size of primary Mg_2Si is as follows: $G > H > E > F > C > A > I > D > B$. Using the average particle size of primary Mg_2Si as the evaluation index, the optimal levels for each factor are determined to be: $A_4B_3C_3D_2E_3F_4G_3H_4I_2$. This means that the first stage of the solid solution temperature should be 460 ℃, the first stage of the aging temperature should be 60 min, the second stage of the solid solution temperature should be 530 ℃, the secondary solid solution time should be 45 min, the quenching medium should be salt solution, the primary aging temperature should be 180 ℃, the primary aging time should be 180 min, the secondary aging temperature should be 195 ℃, and the secondary aging time should be 120 min.

From Fig. 3, it can be observed that the hardness value and the average particle size of incipient

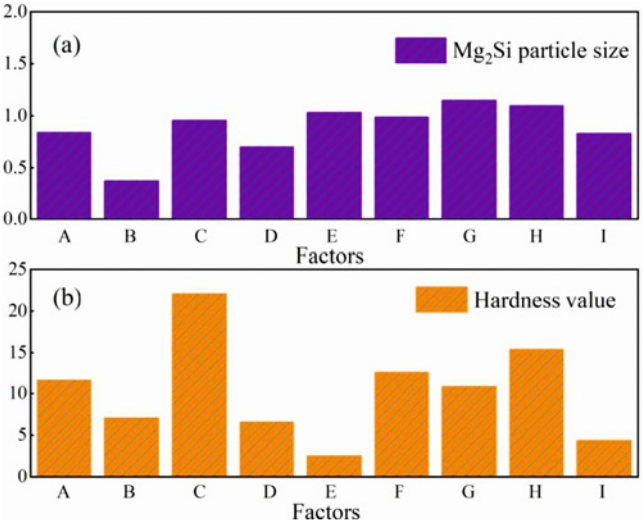

Fig. 4. Range map of each factor concerning the evaluation indicator.

Mg_2Si in the 0.5%Sb-modified 15%Mg_2Si/Al-8Si alloy are primarily influenced by the temperatures of primary and secondary solid solution and aging. The secondary solid solution and secondary aging temperatures exert the most significant impact among these factors. Temperature is the most important factor affecting the diffusion coefficient, by the Arrhenius-type equation, Eq. (3) [32]:

$$D = D_0 \exp\left(-\frac{Q}{RT}\right), \tag{3}$$

where D is the diffusion coefficient, D_0 is the diffusion constant, T is the absolute temperature, Q is the diffusion activation energy, and R is the universal gas constant. The diffusion rate increases as the temperature rises. As the secondary solid solution temperature increases, the hardness value of the alloy gradually improves, and the particle size of the primary Mg_2Si decreases. These effects reach their peak at 530 ℃, after which the hardness decreases and the primary

Table 5. Optimum heat treatment parameters

Factor	*A*	*B*	*C*	*D*	*E*	*F*	*G*	*H*	*I*
Optimum parameter	460 °C	60 min	530 °C	60 min	salt solution	180 °C	180 min	180 °C	120 min

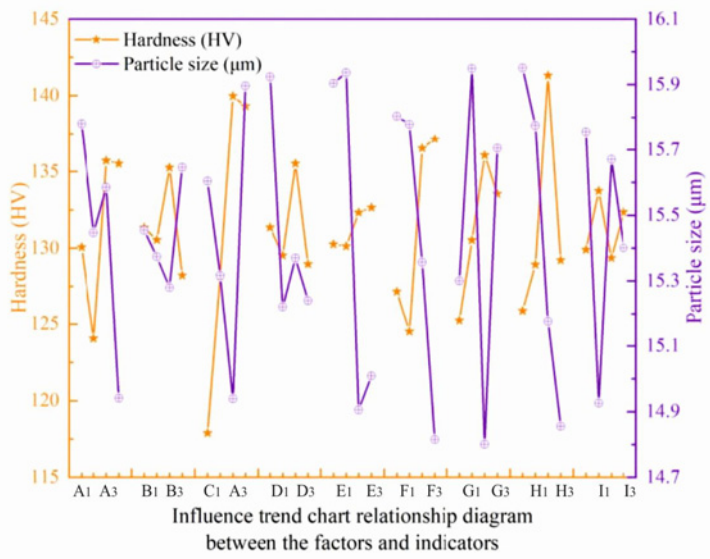

Fig. 5. Influence trend chart relationship diagram between the factors and indicators.

Mg_2Si phase coarsens with further temperature increase. As the secondary aging temperature increases, the hardness value of the alloy gradually improves, and the particle size of primary Mg_2Si decreases. The hardness value reaches its peak at 180 °C, decreasing with further temperature increase. However, the particle size of primary Mg_2Si continues to decrease. The secondary solid solution temperature and secondary aging temperature significantly impact the precipitation of di-phase particles during the heat treatment process. Among the specimens, Specimen 3# demonstrates the most favorable heat treatment effect as its secondary solid solution temperature and secondary aging temperature are at the optimum level. This results in a hardness value of 163.86 HV and primary Mg_2Si particle size refined to below 14 μm. Through an intuitive analysis of the changing trend between the factors and indicators, as depicted in Fig. 5, it is observed that the highest hardness value and the smallest primary Mg_2Si particle size coincide with the optimal level of each factor. This information can be directly obtained. The optimal heat treatment process parameters can be determined by comprehensively considering the hardness value and average size of the primary Mg_2Si particles. These optimized parameters are presented in Table 5, obtained through the orthogonal test of $L_{32}(4^9)$.

3.2. Hardening mechanism of alloys

During the solid solution treatment process, the duration of solid solution time significantly influences the size and morphology of alloy grains, the extent of solid solution for strengthening elements, and the quantity and size of precipitates formed by the second phase after aging. As the solid solution temperature rises, the degree of supersaturation in the solid solution also increases, resulting in a higher driving force for phase transition. This, in turn, reduces the critical nucleation size of aging precipitation and increases the nucleation rate, ultimately enhancing the strengthening effect. From Fig. 3, it is evident that the heat treatment caused a transformation in the shape of the primary Mg_2Si within the alloy. It changed from irregular polygonal to regular massive with a uniform distribution. Additionally, the grain structure of the alloy was refined as well. The process parameters of specimens 3# and 12# are closer to the optimal heat treatment conditions, resulting in good mechanical properties and smaller primary Mg_2Si. In specimen 3#, the secondary solid solution temperature is optimal, while in specimen 12#, the secondary aging temperature is slightly lower. This lower temperature slightly reduces the heat treatment effect due to the lack of elemental diffusion power. When the alloy is subjected to a secondary solid solution temperature of 530 °C, the driving force for recrystallization is higher. This temperature allows for the solid solution of alloying elements such as Mg and Si in the alloy matrix, resulting in solid solution strengthening. The presence of solute atoms and solvent atoms with different diameters results in the formation of lattice distortion around the solute atoms. This distortion acts as a hindrance to dislocation movement, making slip difficult to occur. As a result, the hardness of the alloy is increased. The variation in hardness in the alloy is closely tied to the precipitation state of the second phase. It has been observed that the secondary aging temperature of 180 °C is optimal for promoting an increase in both the number and size of the precipitated phases, resulting in an optimal enhancement in hardness. At lower aging temperatures, the precipitation of the second phase in the alloy is incomplete, resulting in a decrease in the alloy's hardness. In the following sections, the hardening mechanism of the alloy will be further investigated using 3# and 12# specimens.

As observed in Fig. 2 of the metallographic picture, the original as-cast 0.5%Sb-metamorphosed Al-

-15%Mg_2Si-8Si alloy (0#) exhibited a dendritic distribution of α-Al. The incipient Mg_2Si phase was coarse, massive, and fragmented, with irregular shapes and sharp edges and corners. An aggregation phenomenon was observed, resulting in uneven distribution within the aluminum matrix. The eutectic structure was also found to be aggregated and distributed along the boundaries of the α-Al matrix. In specimen 3, the primary Mg_2Si phase appears finer and more uniformly distributed. It exhibits a better-rounded shape with white coils inside, giving the appearance of dividing a particle into multiple small cells. The eutectic structure is also finer in comparison, displaying a fishbone distribution or diffuse distribution pattern. Furthermore, the α-Al phase appears very clean and bright, with a labyrinthine distribution. Primary Mg_2Si of 12# is finer but slightly agglomerated in distribution; the angles are a bit sharp and may cut the matrix, and internally white coils are dividing a particle into several cellular shapes; the eutectic organization is finely striated, herringbone, and diffusely distributed; and α-Al is dendritic in distribution, with the presence of secondary dendrites, which are not as bright. The grain size distributions of the specimens (0#, 3#, 12#) before and after heat treatment are statistically presented in Fig. 6. After heat treatment, the organizations of the 3# specimen and 12# specimen were optimized, and their incipient Mg_2Si was effectively refined, and its distribution was more uniform.

Al-Mg-Si alloys are age-hardening alloys, primarily consisting of Mg and Si as alloying elements. In these alloys, the precipitation order is typically considered to be as follows: [33]: SSSS $\rightarrow$ atomic clusters $\rightarrow$ GP zones $\rightarrow$ β'' $\rightarrow$ β', U1, U2, B′ $\rightarrow$ β, Si. Figure 7 displays the X-ray diffractograms of specimens 0#, 3#, and 12#. The diffractograms reveal the presence of various phases, including the Mg_3Sb_2 phase, $Al_{12}Mg_{17}$ phase, $AlMg_4Si_6$ phase, and the matrix Al and β and Si reinforced phases. After undergoing solid solution and aging treatment, two primary precipitation phases are observed in the alloy: the Mg_2Si equilibrium phase and the massive single-crystal Si phase. These phases exhibit a more uniform distribution throughout the alloy. The purpose of solid solution treatment is to dissolve the Mg_2Si phase and impurity elements that have precipitated during the solidification of the liquid metal into the α-Al matrix. This incorporation allows the alloy to form finer precipitated reinforcing phases from the supersaturated solid solution during aging, ultimately enhancing the strength of the alloy. Additionally, the solid solution treatment can lead to the dissolution and refinement of the coarse Mg_2Si phase and other secondary phases present in the alloy. This process helps reduce the presence of secondary phase prongs and corners within the matrix and mitigates stress concentration caused by these secondary phases. Furthermore, the fine second phase and impu-

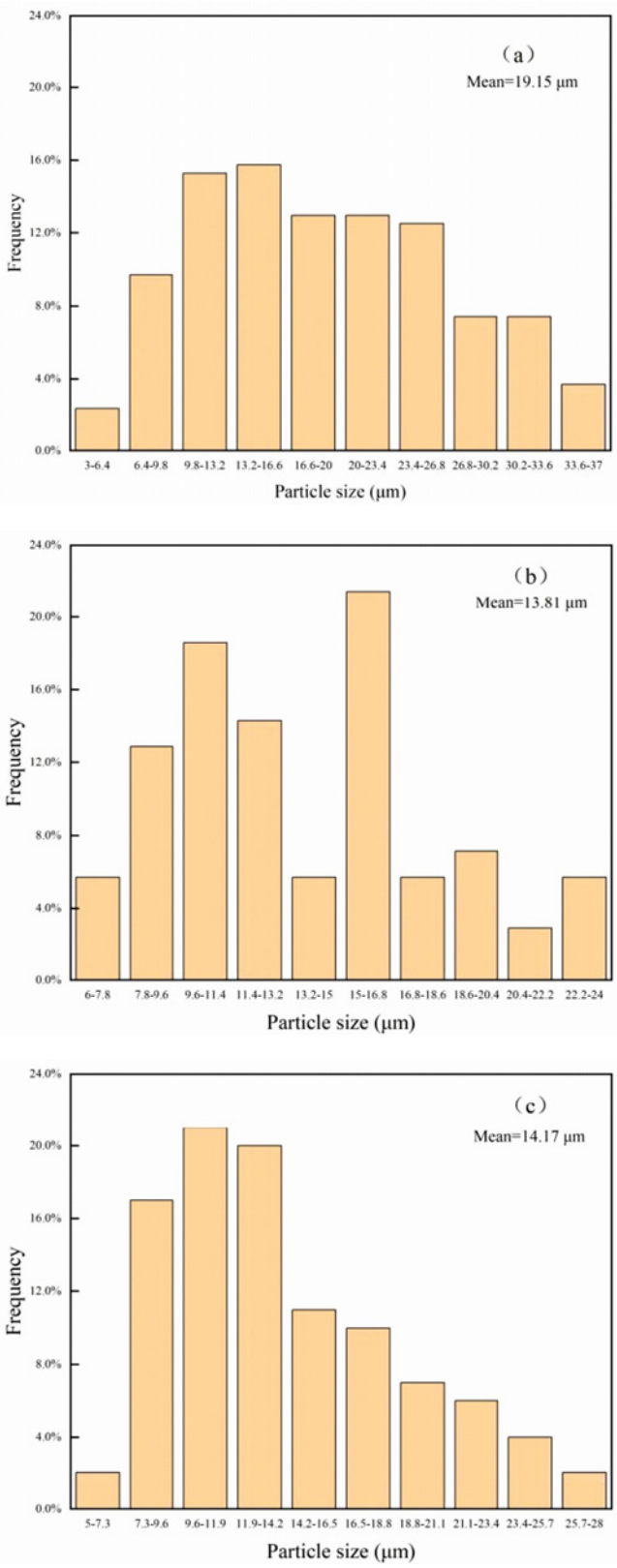

Fig. 6. Particle size distribution histogram of primary Mg_2Si: (a) 0#, (b) 3#, and (c) 12#.

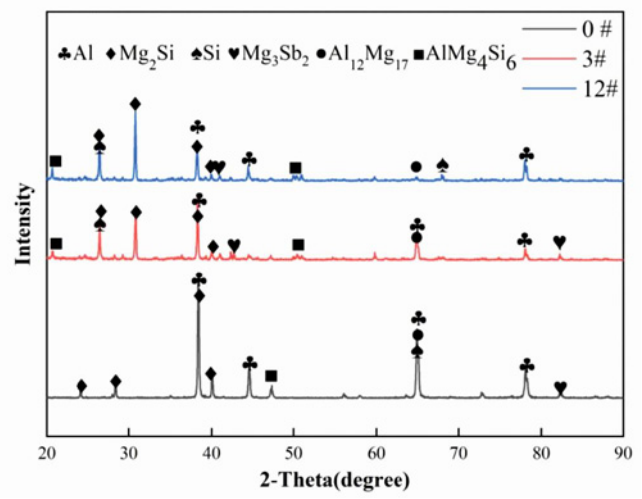

Fig. 7. XRD pattern of the samples 0#, 3#, and 12#.

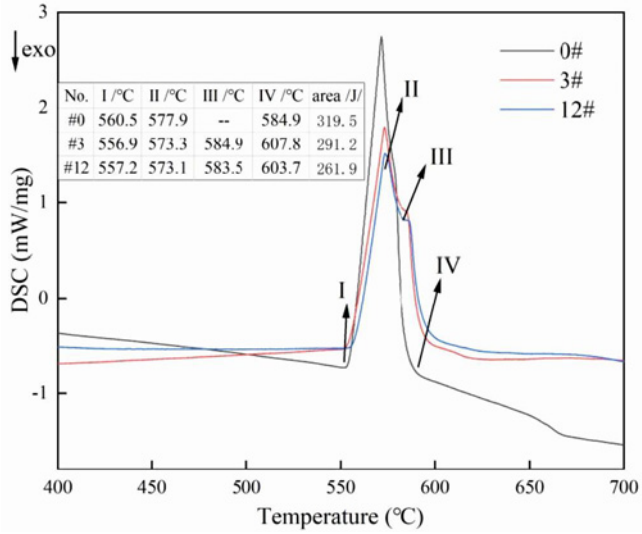

Fig. 8. DSC curves of the sample 0#, 3#, and 12#.

rity phases can be dissolved into the matrix, forming a supersaturated solid solution. The grain growth process observed during the heat treatment of the $L_{32}(4^9)$ orthogonal experiment designed for this study aligns with the grain growth model proposed by Kopp R. et al. [34], as demonstrated in Eq. (4):

$$d_1 = d_0^m \lambda t \exp\left(-\frac{Q_1}{RT'}\right), \tag{4}$$

where d_1 is the grain size, d_0 is the initial grain size, λ and m are material constants, t is time, Q_1 is the free diffusion activation energy, and T' is the solid solution temperature. The observation reveals that the grain growth process during heat treatment is predominantly influenced by the solid solution temperature and the duration of the solid solution treatment. Higher solid solution temperatures and longer solid solution times result in larger grain sizes following the solid solution treatment. At a secondary solid solution temperature of 530 ℃, the microstructure of the alloy benefits from the higher solid solution temperature as it provides sufficient energy for the dissolution of Mg_2Si co-crystalline compounds into the matrix. Subsequently, the dispersed precipitation of β-phase particles occurs during aging, resulting in a more homogeneous microstructure. Consequently, the specimen exhibits improved comprehensive mechanical properties. Figure 7 illustrates that the area occupied by the Mg_2Si phase and single-crystal Si phase in the heat--treated 3# and 12# specimens is noticeably larger than in the 0# specimen. Additionally, the diffraction peaks appear broader, implying that the heat treatment significantly enhances the dissolution and precipitation of Mg_2Si co-crystalline compounds, leading to their refinement. This observation is further supported by Fig. 6. The hardness is usually proportional to the yield strength, so according to the Hall-Petch equation, the Vickers hardness and yield strength are related to the grain size and the interlayer spacing, which can be calculated from Eq. (5) [35]:

$$\sigma_y = \sigma_0' + k_{lm}\lambda^{-\frac{1}{2}} + k_{gb}d^{-\frac{1}{2}}, \tag{5}$$

where σ_0' is the intrinsic frictional stress, d is the grain size, λ is the interlayer spacing, and k_{gb} and k_{lm} are Hall-Petch slope constants related to grain strength and laminated interface strength, respectively. The smaller the grain diameter (d), the higher the yield load (σ_y). This indicates that after heat treatment, the incipient Mg_2Si phase undergoes refinement, resulting in a significant improvement in the hardness of the alloy. The developed DSC processes for 0#, 3#, and 13# samples, which are performed at a heating rate $\alpha = 20\,\mathrm{K\,min^{-1}}$, have been explained in Fig. 8. As shown in Fig. 8, there are mainly four peaks in the range of 400–700 ℃, of which peaks I and IV are exothermic, and peaks II and III are heat-absorbing peaks. Peak I indicates the precipitation of the intermediate phase caused by Mg-Si clusters. Peak II in the graph corresponds to a temperature phase transition that aligns with the melting of the Al-Si eutectic. This finding is consistent with the temperature indicated by the binary Al-Si phase diagram, which is 577 ℃. The temperature information from the Al-Si phase diagram is depicted in the figures. Peak III is attributed to the precipitation of Mg_3Sb_2 particles, which are influenced by heat treatment. Additionally, peak IV corresponds to the melting temperature of α-Al. After heat treatment, the energy absorbed by the alloy (peak II, peak III) is lower compared to the as-cast pristine samples. This can be attributed to the solid solution and aging treatment, which reduces the energy required for melting and promotes the precipita-

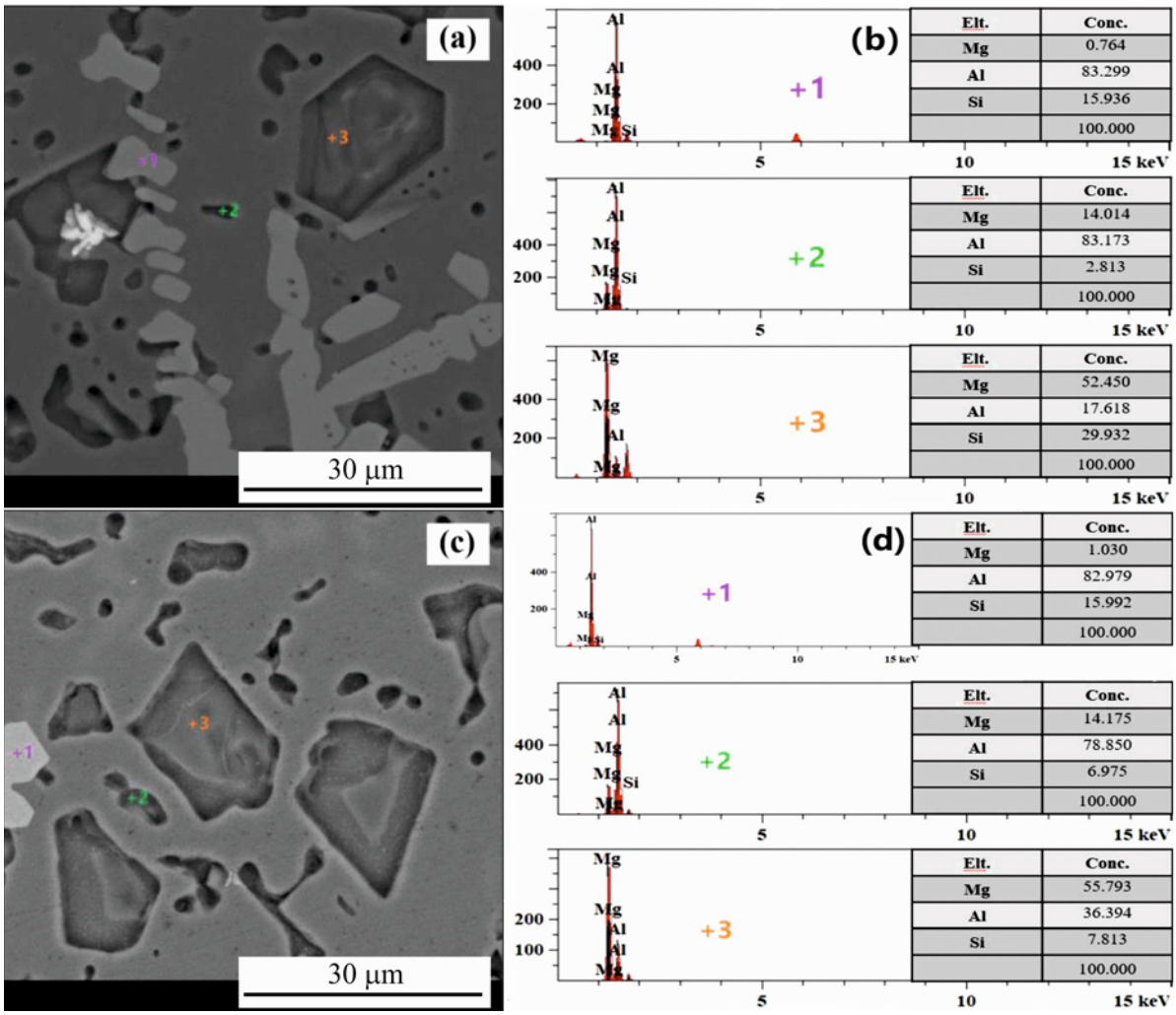

Fig. 9. The SEM and EDS results of alloy specimens: (a) and (b) 3#, (c) and (d) 12#.

tion of Mg_2Si particles. As a result, the energy needed is reduced, making the crystallization reaction more likely to occur.

The hardness of a material is not only influenced by its microstructure but also by the content and uniform distribution of its elements. Figure 8 displays the SEM morphology and corresponding EDS analysis of specimens 3# and 12#. It is evident that the incipient Mg_2Si in specimen 3# tends to be more rounded compared to that of specimen 12#. This characteristic makes the material less susceptible to brittle cracking and enhances the hardness of the alloy. By utilizing EDS analysis, it has been observed that all eutectic tissues at position 1 are enriched with Si elements. Similarly, eutectic tissues at position 2 are biased towards Mg elements. Additionally, at position 3, the incipient Mg_2Si phase dominates the microstructure. The aging process plays a crucial role in driving the precipitation of the second phase in a material. Higher aging temperatures lead to a faster decomposition of the supersaturated solid solution, resulting in an accelerated precipitation of the second phase. In other words, increasing the aging temperature increases the rate of the precipitation process. As the secondary aging temperature increases, the hardness value of the alloy initially increases and then decreases, reaching its peak at 180 ℃. Subsequently, the hardness value of the alloy starts to decrease as the secondary aging temperature continues to rise. With the increase in aging temperature, the concentration of Mg and Si elements in the alloy will further increase. At the peak of specimen 3#, the precipitation of the Mg_2Si strengthened phase reaches an optimal state in terms of quantity, size, and distribution, resulting in an ideal matching condition. The depletion of Mg and Si elements mainly occurs during the formation of the incipient Mg_2Si phase. The 12# sample did not reach the peak temperature, resulting in a slightly slower solute atom diffusion rate. As a result, the precipitation phase did not reach its optimal state. Some eutectic phase precipitates are still present, which weakens the strengthening effect of the precipitation phase. The

precipitation of the second phase in the alloy exerts a significant pinning effect on the movement of dislocations. Additionally, the precipitated phase maintains a co-lattice structure with the matrix, leading to a broader range of point distortions within the matrix. This diffusion reinforcement mechanism greatly enhances the hardness of the material.

4. Conclusions

In this experiment, the heat treatment process of a 15%Mg_2Si/Al-8Si alloy alloyed with 0.5%Sb was investigated by conducting orthogonal experiments of $L_{32}(4^9)$.

The following conclusions were drawn:

1. Among the nine factors considered in the designed orthogonal experiments, the secondary solid solution temperature and the secondary aging temperature had the greatest influence on the properties of the 0.5%Sb-metamorphosed 15%Mg_2Si/Al-8Si alloy. The heat-treated alloy exhibited significant improvements, with the hardness value increasing from 74.77 to 163.86 HV and the average particle size of the incipient Mg_2Si refining from 19.15 to 12.44 μm.

2. The optimized heat treatment process involves a primary solid solution temperature of 460 ℃, a primary aging temperature of 60 min, a secondary solid solution temperature of 530 ℃, a secondary solid solution time of 60 min, quenching in a salt solution, a primary aging temperature of 180 ℃, a primary aging time of 180 min, a secondary aging temperature of 180 ℃, and a secondary aging time of 120 min.

3. The structure of the alloy mainly consists of the primary Mg_2Si phase, α-Al phase, and eutectic Mg_2Si phase. The solid solution and aging treatment process helps reduce the energy required for alloy melting, influencing the dissolution and precipitation of solute atoms. This, in turn, affects the number, size, and distribution of the second phase, ultimately leading to an improvement in the hardness of the alloy.

Acknowledgements

This work was supported by the National Natural Science Foundation of China (52261024) and the Guangxi Natural Science Foundation (2023GXNSFAA026374, 2023AB38012).

References

[1] L. M. Qin, P. Tang, S. X. Meng, Effect of Ni addition on the microstructure, conductivities and mechanical properties of as-cast Al-Fe alloys, Journal of Alloys and Compounds 986 (2024) 174160. https://doi.org/10.1016/j.jallcom.2024.174160

[2] P. Tang, J. S. Lu, Y. X. Yang, F. Mo, L. T. Wei, Effect of various Er/Al-Ti-C ratios on microstructure and tensile properties of the as-cast Al-10Si-0.8Fe alloy, Journal of Alloys and Compounds 968 (2023) 172237. https://doi.org/10.1016/j.jallcom.2023.172237

[3] O. Engler, C. D. Marioara, Y. Aruga, M. Kozuka, O. R. Myhr, Effect of natural ageing or pre-ageing on the evolution of precipitate structure and strength during age hardening of Al-Mg-Si alloy AA 6016, Materials Science & Engineering A, Structural Materials: Properties, Microstructure And Processing 759 (2019) 520–529. https://doi.org/10.1016/j.msea.2019.05.073

[4] P. Tang, K. L. Yu, X. H. Mao, Effect of antimony addition on the microstructure modification and properties evolution of hypereutectic Al-Si-Zr alloy, Kovove Materialy-Metallic Materials 61 (2023) 145–159. https://doi.org/10.31577/km.2023.3.145

[5] P. Tang, Q. N. Liu, F. Y. Yu, F. Mo, L. M. Qin, Effect and its mechanism of fixed-ratio and incremented 3Be-Sb complex modifier on microstructures and properties of hypereutectic Al-Si-Mg alloy, Journal of Alloys and Compounds 931 (2023) 167478. https://doi.org/10.1016/j.jallcom.2022.167478

[6] G. Chen, X. S. Chang, J. X. Zhang, Y. Jin, C. Sun, Q. Chen, Z. D. Zhao, Microstructures and mechanical properties of in-situ Al_3Ti/2024 aluminum matrix composites fabricated by ultrasonic treatment and subsequent squeeze casting, Metals and Materials International 26 (2020) 1574–1584. https://doi.org/10.1007/s12540-019-00396-y

[7] Y. Y. Ren, T. Y. Liu, Y. M. Li, H. Hu, Effect of La inoculation on composition, content, granularity and mechanical properties of in-situ Al-30wt%Mg_2Si Composite, Materials Science & Engineering A, Structural Materials: Properties, Microstructure and Processing 704 (2017) 119–127. https://doi.org/10.1016/j.msea.2017.08.010

[8] W. L. Gu, C. X. Lu, P. F. Zhou, Study on microstructure modification of hypereutectic Al-Si alloy by Mg, China Foundry 70 (2021) 921–927.

[9] W. Cheng, C. Y. Liu, H. F. Huang, L. Zhang, B. Zhang, L. Shi, High strength and ductility of Al-Si-Mg alloys fabricated by deformation and heat treatment, Materials Characterization 178 (2021) 111278. https://doi.org/10.1016/j.coco.2022.1010778

[10] Y. H. Zhang, X. Li, Z. B. Yang, H. J. Zhao, H. X. Luo, Effect of predeformation on microstructure and mechanical properties of Al-Mg-Si alloy, Heat Treatment of Metals 43 (2018) 165–169.

[11] Q. Zhou, S. J. Zang, Q. Ma, J. G. Jia, G. L. Xi, A. Liang, Preparation and properties of novel Al/Mg_2Si composites, Nonferrous Metals 59 (2007) 6–13.

[12] Q. X. Jing, X. D. Huang, Study on solidification structure of in-situ autogenous Mg_2Si/A1 matrix composites with different Mg and Si contents, Light Alloy Fabrication Technology 35 (2007) 44–46.

[13] Y. H. Dai, J. X. Chen, X. X. Chu, Effect of Si, Mg content on the performance of A356 aluminum alloy wheels, China Foundry 63 (2014) 257–260.

[14] Z. L. Huang, K. Wang, Z. M. Zhang, B. Li, H. S. Xue, D. Z. Yang, Effects of Mg content on primary Mg_2Si phase in hypereutectic Al-Si alloys, Transactions of Nonferrous Metals Society of China 25 (2015) 3197–3203. https://doi.org/10.1016/S1003-6326(15)63956-5

[15] J. X. Zhang, S. J. Shao, A. H. Gao, Effect of Mg/Si mass ratio on microstructure properties of Al-Mg-Si alloy, Light Metals 32 (2012) 56–59.
[16] J. Y. Li, Q. An, S. S. Wu, F. Li, S. L. Lü, W. Guo, Relationship of Mg_2Si morphology with Mg_2Si content and its effect on properties of in-situ Mg_2Si/Al-Cu composites, Journal of Alloys and Compounds 808 (2019) 151771. https://doi.org/10.1016/j.jallcom.2019.151771
[17] P. Tang, F. Y. Yu, X. D. Teng, L. X. Peng, K. Wang, Effect of beryllium addition and heat treatment on the microstructure and mechanical properties of the 15%Mg_2Si/Al-8Si composite, Materials Characterization 180 (2021) 111416. https://doi.org/10.1016/j.matchar.2021.111416
[18] A. Islahuddin, G. Hamidreza, A. A. B. Tuy, C. Y. Chong, Effect of praseodymium addition on wear properties of Al-15%Mg_2Si composites, Materials Today: Proceedings 39 (2020) 1051–1055. https://doi.org/10.1016/j.matpr.2020.05.204
[19] K. Y. Wang, R. D. Zhao, F. F. Wu, X. F. Wu, M. H. Chen, J. Xiang, S. H. Chen, Improving microstructure and mechanical properties of hypoeutectic Al-Mg_2Si alloy by Gd addition, Journal of Alloys and Compounds 813 (2020) 152178. https://doi.org/10.1016/j.jallcom.2019.152178
[20] R. Khorshidi, A. H. Raouf, R. Mahmudi, Microstructural evolution and high temperature mechanical properties of cast Al-15Mg_2Si-xGd in situ composites, Journal of Alloys and Compounds 700 (2017) 18–28. https://doi.org/10.1016/j.jallcom.2017.01.015
[21] M. R. Ghorbani, M. Emamy, N. Nemati, Microstructural characterization of Al-15%Mg_2Si composites containing chromium, Materials and Design 32 (2011) 4262–4269. https://doi.org/10.1016/j.matdes.2011.04.020
[22] B. Ren, Z. X. Liu, R. F. Zhao, T. Q. Zhang, Z. Y. Liu, M. X. Wang, Y. G. Weng, Effect of Sb on microstructure and mechanical properties of Mg_2Si/Al-Si composites, Transactions of Nonferrous Metals Society of China 20 (2010) 1367–1373. https://doi.org/10.1016/S1003-6326(09)60306-X
[23] P. Tang, F. Y. Yu, Q. N. Liu, Y. L. Xie, L. X. Peng, Z. Q. Mo, Effect of Sb content and heat treatment on microstructure and properties of Al-11.5Si-9.5Mg alloy, Rare Metals 46 (2022) 428–437.
[24] Q. Cai, C. L. Mendis, I. T. H. Chang, Z. Y. Fan, Effect of short T6 heat treatment on the microstructure and the mechanical properties of newly developed die-cast Al-Si-Mg-Mn alloys, Materials Science and Engineering A 788 (2020) 139610. https://doi.org/10.1016/j.msea.2020.139610
[25] Q. L. Liu, Y. Z. Liu, L. Du, X. Luo, J. L. Xie, Heat treatment process of jet forming 6061 aluminum alloy, The Journal of Nonferrous Metals 2 (2012) 350–357.
[26] Z. L. Li, C. Li, Y. C. Liu, L. M. Yu, Q. Y. Guo, H. J. Li, Effect of heat treatment on microstructure and mechanical property of Al-10%Mg_2Si alloy, Journal of Alloys and Compounds. 663 (2016) 16–19. https://doi.org/10.1016/j.jallcom.2015.12.128
[27] A. Malekan, M. Emamy, J. Rassizadehghani, A. R. Emami, The effect of solution temperature on the microstructure and tensile properties of Al-15%Mg_2Si composite, Materials & Design 32 (2011) 2701–2709. https://doi.org/10.1016/j.matdes.2011.01.020
[28] L. Zhen, S. B. Kang, The effect of pre-aging on microstructure and tensile properties of Al-Mg-Si alloys, Scripta Materialia 36 (1997) 1089–1094. https://doi.org/10.1016/S1359-6462(96)00487-3
[29] K. Osman, E. Harun, J. J. O. Taher, G. Mehmet, Determination of solid-liquid interfacial energy of solid Mg_2Si intermetallic phase in equilibrium with liquid AlSiMg eutectic solution in AlSiMg energy storage alloy, Intermetallics 135 (2021) 107235. https://doi.org/10.1016/j.intermet.2021.107235
[30] J. Zhang, Z. Fan, Y. Q. Wang, B. L. Zhou, Equilibrium pseudodobinary Al-Mg_2Si phase diagram, Journal of Materials Science & Technology 17 (2001) 494–496. https://doi.org/10.1179/026708301101510311
[31] C. Li, Y. Y. Wu, H. Li, X. F. Liu, Morphological evolution and growth mechanism of primary Mg_2Si phase in Al-Mg_2Si alloys, Acta Materialia 59 (2011) 1058–1067. https://doi.org/10.1016/j.actamat.2010.10.036
[32] Z. Z. Shang, H. Z. Qi, X. T. Liu, C. Z. Ouyang, Y. S. Wang, Structural optimization of lithium-ion battery for improving thermal performance based on a liquid cooling system, International Journal of Heat and Mass Transfer 130 (2019) 33–41. https://doi.org/10.1016/j.ijheatmasstransfer.2018.10.074
[33] R. L. Ma, C. Q. Peng, Z. Y. Cai, R. C. Wang, Z. H. Zhou, X. G. Li, X. Y. Cao, Manipulating the microstructure and tensile properties of selective laser melted Al-Mg-Sc-Zr alloy through heat treatment, Journal of Alloys and Compounds 831 (2020) 154773. https://doi.org/10.1016/j.jallcom.2020.154773
[34] L. P. Ding, Y. Y. Weng, Z. H Jia, R. J. Zang, K. Y. Xiang, Q. Liu, H. Nagaum, Interactive transformation mechanisms of multiple metastable precipitates in a Si-rich Al-Mg-Si alloy, Philosophical Magazine Part A: Materials Science 102 (2022) 1602–1627. https://doi.org/10.1080/14786435.2022.2051633
[35] K. Karhausen, R. Kopp, Model for integrated process and microstructure simulation in hot forming, Steel Research 63 (1992) 247–256. https://doi.org/10.1002/srin.199200509
[36] S. Yim, H. K. Bian, K. Aoyagi, A. Chiba, Effect of multi-stage heat treatment on mechanical properties and microstructure transformation of Ti-48Al-2Cr-2Nb alloy, Materials Science & Engineering A, Structural Materials: Properties, Microstructure and Processing 816 (2021) 141321. https://doi.org/10.1016/j.msea.2021.141321